RESEARCH

# Partial Male Sterility in Imisun Sunflower: Imazapyr Treatment in Advanced Vegetative Stages Decreases Pollen Yield and Alters *ahas* Gene Expression

Ana C. Ochogavía,* María A. Novello, Marta B. Bianchi, Liliana A. Picardi, and Graciela M. Nestares


## ABSTRACT

Imidazolinones are powerful herbicides that inhibit branched-chain amino acid biosynthesis by targeting the catalytic subunit of acetohydroxyacid synthase (AHAS). Imidazolinone application in the advanced vegetative or early reproductive developmental stages is associated with male sterility in resistant sunflower (*Helianthus annuus* L.); however, the underlying mechanism of this sterility remains unknown. This study describes the morphological, cytoembryological, and molecular alterations induced by imazapyr (IM) treatment on reproductive tissues at different developmental stages in two sunflower genotypes, resistant and intermediate resistant, respectively. Pollen and seed physiological variables were compared between the treated and control plants. The number of pollen grains per flower and viable seeds were negatively affected by IM treatment in the intermediate-resistant genotype, and the biometric traits of early developed disc flower were also significantly different in this genotype. Differential interference contrast microscopy revealed that IM treatment slightly accelerates megagamethophyte development. Anther observations at microsporogenesis using confocal microscopy show that the sporogenous tissue was damaged. Furthermore, the expression profiles of the sunflower AHAS paralogs (*ahas1*, *ahas2*, and *ahas3*) were measured by quantitative polymerase chain reaction in the anthers and pistils of two developmental stages in treated and control plants. Imazapyr treatment in early reproductive growth stages clearly induces divergent expression patterns in the *ahas* gene family. These findings provide new insight into a novel chemical method for inducing male sterility in sunflowers and enhance our understanding of the effects of AHAS-inhibitor herbicides in reproductive tissues.


A.C. Ochogavía, M.A. Novello, L.A. Picardi, and G.M. Nestares, IICAR, UNR, CONICET (Instituto de Investigaciones en Ciencias Agrarias de Rosario, Univ. Nacional de Rosario, Consejo Nacional de Investigaciones Científicas y Técnicas), Campo Experimental 'J.F. Villarino', Zavalla, Santa Fe, Argentina; M.B. Bianchi and L.A. Picard, CIUNR, Consejo de Investigaciones Univ. Nacional de Rosario, Campo Experimental 'J.F. Villarino', Zavalla, Santa Fe, Argentina; M.B. Bianchi, Facultad de Ciencias Agrarias, UNR, Campo Experimental 'J.F. Villarino', Zavalla, Santa Fe, Argentina. Received 12 Dec. 2017. Accepted 18 Apr. 2018. *Corresponding author (anaochogavia@conicet.gov.ar). Assigned to Associate Editor Manjit Kang.

**Abbreviations:** AHAS, acetohydroxyacid synthase; BCAA, branched-chain amino acid; cDNA, complementary DNA; DIC, differential interference contrast microscopy; I, intermediate-resistant sunflower genotype; IM, imazapyr; IMI, imidazolinone; PCR, polymerase chain reaction; PGF, pollen grains per flower; qPCR, quantitative polymerase chain reaction; R, completely resistant sunflower genotype; SSI, sporophytic self-incompatible mechanism.

Acetohydroxyacid synthase (AHAS; EC 4.1.3.18) is the first enzyme in the biosynthesis of the branched-chain amino acids (BCAAs) and is also known as acetolactate synthase (ALS) (Singh and Shaner, 1995). Acetohydroxyacid synthase catalyzes the condensation of two pyruvate molecules to form acetolactate in the leucine and valine pathway. It can also catalyze one molecule of pyruvate with one molecule of 2-ketobutyrate to form 2-aceto-2-hydroxybutyrate as the first step in the isoleucine biosynthesis (Singh and Shaner, 1995). Major interest in AHAS has developed since the herbicides sulfonylurea and imidazolinone (IMI) were discovered as enzyme inhibitors (LaRossa and Schloss, 1984; Ray, 1984). Knowledge about their modes of action has helped to explain why these herbicides have very low toxicity in animals. Acetohydroxyacid synthase is not present in animals, but it has been detected in

Published in Crop Sci. 58:1–14 (2018).
doi: 10.2135/cropsci2017.12.0726

all plant samples measured thus far and in some microorganisms (Duggleby et al., 2008).

Acetohydroxyacid synthase is the target site of five structurally diverse chemical classes: sulfonylureas, IMIs, triazolopyrimidines, pyrimidinylthio- (or oxy-)benzoates, and sulfonylamino-carbonyltriazolinones (Tan et al., 2006). These classes of herbicides are absorbed by the roots and foliage and then transported into the meristems of the plants. They inhibit AHAS by blocking substrate access to the active sites by binding within the substrate-access channel, and the inhibition is noncompetitive with pyruvate (Duggleby et al., 2008).

The inhibition of AHAS leads to a global elevation of free amino acid levels and imbalances in their relative proportions (Hofgen et al., 1995). Crop injury after herbicide treatment includes symptoms such as chlorosis, stunting, yellowing, reduction of biomass production, and yield loss. Spontaneous resistance to AHAS-inhibiting herbicides has been discovered in many wild populations of crops and weeds exposed to strong selection pressure from herbicide (Gressel and Segel, 1978; Mallory-Smith et al., 1990). Acetohydroxyacid synthase inhibitory resistance either is manifested as a consequence of enhanced metabolism of the herbicide by the plant or it is due to the mutation of the AHAS gene, which in turn results in the change of a single amino acid residue in the herbicide-binding site (Tranel and Wright, 2002). Sunflower (*Helianthus annuus* L.) is the second most important oilseed crop in the world. Similar to other annuals in the same genus, this species is an outcrosser that bears a sporophytic self-incompatible mechanism (SSI) (Heiser et al., 1969) where the pollen grain phenotype is determined by the diploid genotype of the anther from which it originates (Hiscock and McInnis, 2003). Nevertheless, in cultivated sunflower, breeding for self-compatibility has been very successful, achieving 15 to 95% self-compatibility with an average of 68% (Astiz et al., 2011).

The flowers of *H. annuus* are arranged in a capitulum that consists of an outer whorl of asexual ligullate flowers in the peripheria and inner whorls of bisexual flowers in the disc. The individual disc flowers develop sequentially, with flowers from the outer whorls developing before those in the center of the inflorescence. Bisexual flowers present dicogamy and are protandious, which means that anthers dehiscence first occurs with pollen release, followed by receptivity of the bilobate stigma.

The first commercial herbicide resistance trait in sunflower was introgressed into elite inbred lines by conventional breeding methods to develop IMI-resistant cultivars known as Imisun sunflowers (Miller and Al-Khatib, 2002; Sala et al., 2012). A digenic model adequately explained the inheritance of Imisun, where a major nuclear inherited semidominant gene (*Imr1*) interacts with a second modifier gene (*Imr2*) to confer complete resistance (Bruniard and Miller, 2001). Therefore, complete resistance in sunflower hybrids can only be achieved by homozygosity of both resistant genes in parental lines (Bruniard and Miller, 2001).

Catalytic subunits of AHAS are coded by three different nuclear genes: *ahas1*, *ahas2*, and *ahas3*. *Ahas1* is a multiallelic locus and the only member of this gene family where all the induced and natural mutations for herbicide resistance in sunflower have been described (Kolkman et al., 2004; Sala et al., 2012). The gene *Imr1*, also known as *Arpur* (Kolkman et al., 2004) or *Ahasl1-1* (Sala et al., 2008), harbors a C-to-T mutation in codon 205, which confers a moderate resistance to IMI. Our group findings revealed that the mechanism of resistance endowed by modifier gene *Imr2* is related to non-target-site resistance (Breccia et al., 2017). We also have identified, in previous gene expression studies, that the three *ahas* paralogs are tissue specific and temporarily regulated (Ochogavía et al., 2014). The maximum expression of *ahas2* and *ahas3* occurred in bud flowers and embryos, and the highest expression of *ahas1* was detected in young leaves (Ochogavía et al., 2014).

Chemical hybridization agents could be used to induce male sterility for the production of hybrid seeds. The AHAS-inhibitory hybridization agent used in rapeseed (*Brassica napus* L.) is tibenuron methyl. Recently published results have associated this treatment with anomalous microsporogenesis. Zhao et al. (2015) proposed that BCAA starvation induces pollen formation failure and ultimately leads to autophagic cell death in the anthers. In sunflower, it has been reported as a promising method for producing male sterility by IMI treatment (Sala and Bulos, 2012). The application of imazethapyr during the early reproductive development stages induced male and female sterility in IMI-resistant sunflower lines.

Male sterility induced by herbicide treatment could allow breeders to test the combining ability of sunflower maintainer lines in the early stages of development, as well as provide flexibility in the application timing of breeding programs. However, no evidence about the underlying mechanism by which this herbicide interferes with the normal development of reproductive tissues is available in sunflower. The aim of this work was to characterize the reproductive tissue development of two Imisun genotypes, as well as the expression patterns of the three *ahas* paralogs in the stamens and pistils of plants treated with IM in the early reproductive growth stages. The results provide knowledge about a new method to produce male sterility in sunflower and contribute to the understanding of the molecular effects of AHAS-inhibitor herbicides in reproductive tissues.

# MATERIALS AND METHODS

## Plant Materials and Growth Conditions

Two inbred, Imisun sunflower lines were used in this study—HA425 (*Imr1 Imr1 Imr2 Imr2*) and 1058-1 (*Imr1 Imr1 imr2 imr2*), which are IMI resistant (R) and intermediate resistant (I), respectively. The HA425 line was developed and released by the USDA-ARS and the North Dakota Agricultural Experiment Station (Miller and Al-Khatib, 2002), and the 1058-1 line was developed from a backcross between HA425 and an IMI-susceptible line HA89 (Bruniard and Miller, 2001).

Plants were grown conventionally at the Experimental Field Station of Universidad Nacional de Rosario (33°1′ S, 60°53′ W) with careful exclusion of insects and weeds in a completely randomized design with six replications. Each replication included 20 plants. The commercial herbicide imazapyr (IM) was used {2-[(*RS*)-4-isopropil-4-metil-5-oxo-2-imidazolin-2-il] nicotinic acid; Clearsol, BASF}. The herbicide was applied at a dose of 80 g a.i. $ha^{-1}$ when plants were in the R1 early reproductive developmental stage (Schneiter and Miller, 1981), as described by Sala and Bulos (2012). Cross-pollination was prevented by covering inflorescences with pollination bags. Field experiments of lines HA425 and 1058-1 were performed in the 2015–2016 and 2016–2017 seasons, respectively. The assay including both genotypes was repeated in season 2017–2018 to obtain the samples for the confocal microscopy analysis. All statistical comparisons were conducted between treated and control plants of each genotype.

Five reproductive tissue samples were randomly obtained from different plants of each replication. Flower buds were dissected from capitula 11 d after treatment and also in different stages of development when the complete plant achieved the R5 developmental stage, including (i) completely closed bud flowers (E1 phenophase) and (ii) flowers in anthesis (E3 phenophase) (Schneiter and Miller, 1981) from both the treated and control plants. Stamens (male tissues) and ovaries (female tissues) were dissected from flowers and immediately frozen at −80°C in separate microtubes until RNA extraction. The anthers and ovaries used in the cytoembryologycal study were fixed for 24 h in modified FAA, which contained 95% ethanol, glacial acetic acid, distilled water, 40% formaldehyde, and 25% glutaraldehyde GII in proportions of 50:5:35:8:2 (Lersten and Curtis, 1988).

## Morphological Characterization of Disc Flowers

Digital stereomicroscope images of five bisexual disc flowers from five independent plants were obtained under an SZM-LED2 microscope (OPTIKA Microscopes Italy) from each combination of genotype (R and I), phenophase (E1 and E3), and IM treatment (IM-treated and control) ($n = 200$). Different morphological parameters were measured from photographs using ImageJ software (Abramoff et al., 2004): total flower length, ovarian length, and ovarian width. Data were tested for equal variance using Levene's test and for normality using a Shapiro–Wilk test at the 5% significance level. Statistical differences were determined by pairwise comparisons of treated and control plants of each genotype with a Student's $t$ test ($p < 0.05$) using R version 3.0.0 (R Development Core Team, 2013).

## Quantitative and Qualitative Pollen Grain Analyses

The number of pollen grains per flower (PGF) was estimated using a haemocytometer Improved Neubauer-Boeco on five closed flowers (in phenophase E1) from three different treated and control plants of each genotype (total number of samples = 60) (Kearns and Inouye, 1993). One anther per flower was carefully dissected. The pollen content of the lower half of the right theca was removed and placed in a 0.2-mL microtube with 30 μL of distilled water. The contents were stirred in a vertical vortex mixer to achieve a homogeneous suspension of pollen. A 5-μL aliquot from the pollen suspension was transferred to a Neubauer haemocytometer slide, and the grains were counted under a SZM-LED2 (OPTIKA Microscopes Italy) stereomicroscope, and it was used to estimate the total pollen contained in the original suspension (Kearns and Inouye, 1993). The number of pollen grains per anther was calculated as the product between the counted pollen grains in the suspension and the four anther quarters. Finally, the PGF was calculated by multiplying the number of anthers per flower (normally five) by the number of pollen grains per anther.

To assess viability, fresh pollen was collected on a glass slide during the anther dehiscence period (E3 phenophase) and was immediately soaked in a solution of lactophenol and 0.01% aniline blue (w/v) (Maneval, 1936). The dye allows for discrimination between viable and nonviable pollen grains, as it is capable of incorporating into the cytoplasm in only permeable cells. Blue-stained grains typically have high germination rates (Maneval, 1936). Stained and nonstained pollen grains were counted under the SZM-LED2 stereomicroscope from a total of 100 grains per plant from five treated and control plants, and the viability percentages were calculated.

The pollen grain diameter and the exomorphology were investigated using differential interference contrast (DIC) microscopy. The tissue clarification method was based on Herr's clearing solution (lactic acid, chloral hydrate, phenol, clove oil, and xylene; ratio of 2:2:2:2:1) for Nomarski interference contrast optics (Herr, Jr., 1971). The anthers of five flowers in anthesis from three different treated and control plants of each genotype were dissected under the SZM-LED2 stereomicroscope and soaked in the Herr's solution using cavity microscope slides.

Pollen grains were analyzed under DIC microscopy with a Leica DM2500 microscope (Leica Microsystems) equipped with 10×, 20×, and 40× HI PLAN achromat objectives. Images were digitalized using Leica Application Suite 4 software (Leica Microsystems, 2009). The diameters of five PGF ($n = 300$) were measured from the innermost layer of the pollen grain exine using ImageJ 1.48 (Abramoff et al., 2004). The equal variance and normality of the empirical distribution of all variables was assessed by Levene's and Shapiro–Wilk test, respectively. For each genotype mean values from the treated and control plants were statistically compared by Student's $t$ test ($p < 0.05$) in R version 3.0.0 (R Development Core Team, 2010).

A supplemental study was conducted from three fixed young capitula (11 d after treatment) per treatment combinations in R and I genotypes. Immature reproductive tissue was fixed in modified FAA as was described above and dissected under a binocular SZM-LED2 stereomicroscope. Five anthers from different flowers were clarified using Herr's solution (Herr,

Jr., 1971). They were analyzed under confocal microscopy and imaged on No. 1.5 cover slips. All images were collected with a C1plus confocal on a Nikon TE2000 E2 inverted microscope (Nikon Instruments) equipped with 20× Plan Apo numerical aperture 1.0 objective. Green fluorescence with the 488-nm line from a 40 mW Melles Griot argon ion laser and a 525/50 emission filter. Images were acquired with Nikon EZ-C1 version 3.9 software (Nikon Corporation, 2009).

## Megagametophyte Development

Pistils from disc flowers at two different developmental stages (E1 and E3 phenophases) were fixed in modified FAA (Lersten and Curtis, 1988). Ovules were carefully dissected from ovaries and clarified by Herr's technique (1971) using cavity microscope slides, as described above. Three ovules of three different treated and control plants from each genotype were observed by DIC microscopy with a Leica DM2500 microscope (Leica Microsystems) equipped with 10×, 20×, and 40× HI PLAN achromat objectives. Images were digitized and cellular structures were measured using Image*J* 1.48 (Abramoff et al., 2004). Ovule and embryo sac structures are indicated in Supplemental Fig. S1. The embryo sac's length and width and the nucellar–endothelium layer's width in the broader section of the embryo sac were measured. The equal variance and the normality of empirical distribution of all variables were assessed by Levene's and Shapiro–Wilk test, respectively. For each genotype, mean values of treated and control plants were statistically compared using a Student's *t* test in R version 3.0.0 (R Development Core Team, 2010).

## Filled Seed Count

Mature seeds from five treated and control plants of each genotype were analyzed by hand. A total of 100 seeds per plant were soaked in distilled water until the pericarp could be easily removed. The presence of vital seed structures such as cotyledons and radicles were verified. Empty, partially empty, and normal seeds were classified. The number of filled seeds was recorded for R and I genotypes ($n$ = 2000). The equal variance and the normality of the empirical distribution was assessed by Levene's and Shapiro–Wilk test. The mean values of treated and control plants were statistically compared with Student's *t* test using R version 3.0.0 (R Development Core Team, 2010).

## RNA Extraction and Complementary DNA Synthesis

The RNA was extracted from 120 to 150 mg of anthers and ovaries using a PureLink RNA Mini Kit (Invitrogen Life Technologies) according to the instructions provided by the manufacturer. Two independent RNA extractions were performed from each tissue. DNase I treatment was performed using PureLink DNase with column application (Invitrogen Life Technologies). The RNA integrity was verified on 1% agarose gel and stored at −80—C until use. First-strand complementary DNA (cDNA) synthesis was performed using the SuperScript First-Strand Synthesis System for real-time polymerase chain reaction (PCR, Invitrogen Life Technologies) according to the manufacturer's instructions. Reverse transcription was initiated using oligo(dT) supplied by the kit. The cDNA was diluted at 1:5 using nuclease-free water. A detailed description of the experimental procedure is provided in Supplemental Table S1.

## Quantitative PCR Analysis

Three *ahas* genes (*ahas1*, *ahas2*, and *ahas3*) and three reference genes (*Actin*, *MicroRNA precursor 156*, and *Unknown protein 2* as *ACT*, *MIR156*, and *UNK2* ,respectively) were amplified by real-time PCR using a Rotor-Gene Q with high-resolution melting thermal cycler (Qiagen). The oligonucleotides sequences of the *ahas* genes have been previously designed and assayed by our group and published in Breccia et al. (2013). The reference genes has also been selected and validated by our research group (*ACT*, *MIR156*, and *UNK2*) and were published as the optimal reference panel for reproductive tissue expression normalization of *H. annuus* (Ochogavía et al., 2017). The primers and amplification conditions are available in Ochogavía et al. (2017).

Three technical replicates from each tissue were assayed from two independent plants. The reaction medium contained 1× SYBR Green PCR Master Mix (Mezcla Real, Biodynamics), 0.4 μM of the forward and reverse primers, and 3 μL of cDNA in a total volume of 15 μL. An initial denaturalization step was included (2 min at 70°C), followed by 40 cycles consisting of denaturation for 15 s at 95°C, annealing for 30 s at 58 to 61°C, and extension for 40 s at 72°C. No-template controls were also included.

The quantitation cycle (Cq) and efficiency values ($E$) of each independent quantitative PCR (qPCR) run were obtained from the Comparative Quantitation application of Rotor-Gene Q Series software (QIAGEN, 2008). The primer amplification specificity was verified for the existence or lack of primer dimers or nonspecific amplicons by the presence of a single peak in qPCR melting curve products and the presence of a single band of the expected size on 2.5% agarose gel. A checklist outlining the RNA to qPCR quality and methodology is presented in the Supplemental Table S1. Each replicate sample value was normalized by the three previously validated reference genes.

The relative profiling of each *ahas* gene was compared among tissues and developmental stages in treated and control plants using qBASE+ software version 3.1 (Hellemans et al., 2007). Additionally, differences in relative expression were tested for statistical significance between treated and control plants and between the two developmental stages using the Relative Expression Software Tool (REST) version 2.0.13 (Pfaffl et al., 2002). Transcript levels were referenced to the lowest gene expression. The results of both analysis methods were also compared.

# RESULTS

## Morphological Characterization of Disc Flowers

Plants of the inbred lines HA425 (R) and 1058-1 (I) treated with IM did not show any herbicidal effect in leaves or buds, and they achieved flowering on the same date as the control plants (Fig. 1A–1D). Imidazolinone-susceptible treated plants (inbred line HA89) showed immediate dehydration symptoms (24 h after application)

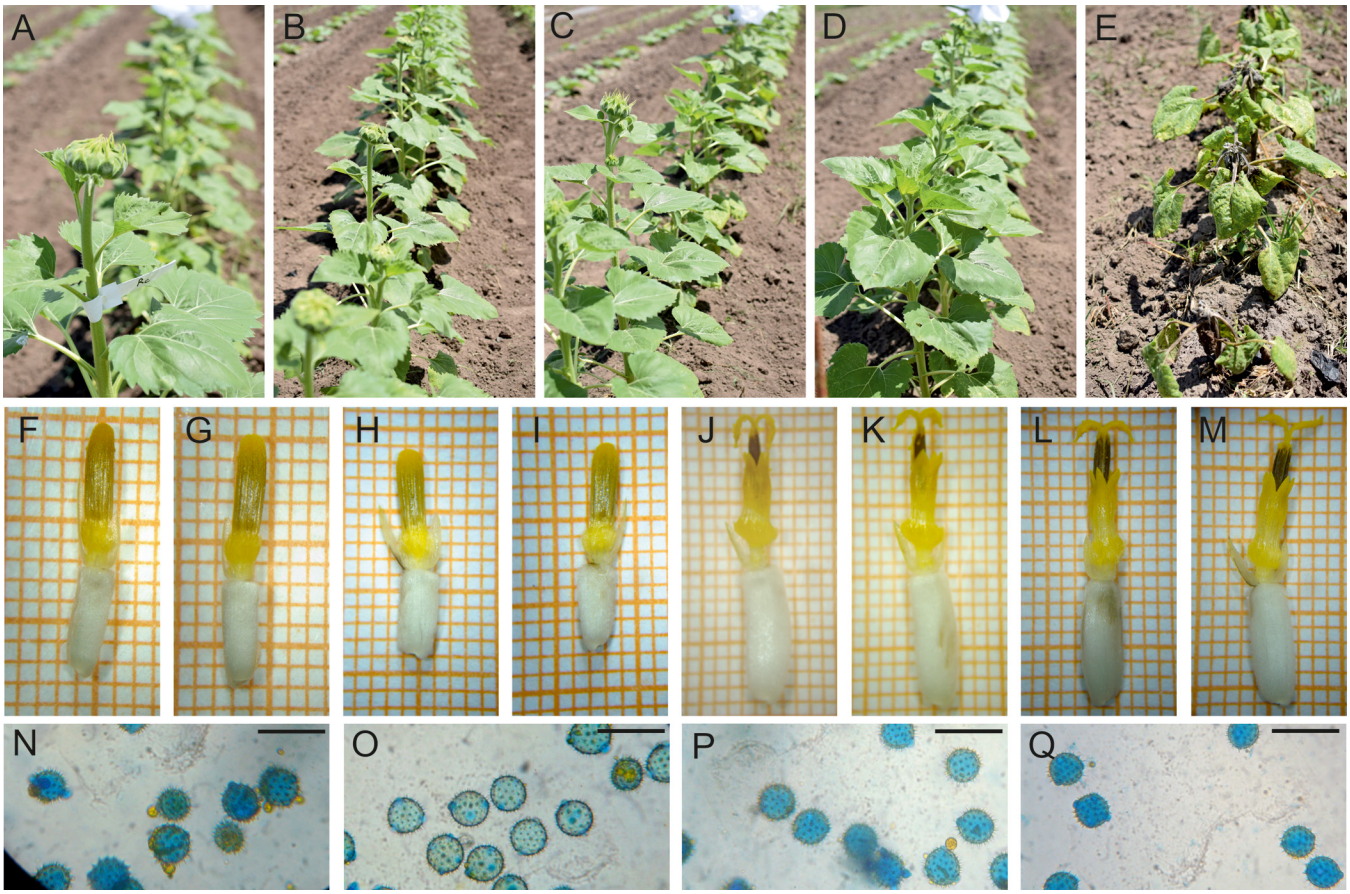


Fig. 1. Comparison of imazapyr-treated (IM-treated) and control plants from HA425 imidazolinone-resistant (R) and 1058-1 intermediate-resistant (I) genotypes. Plants in the field belong to: (A) R control and (B) R IM-treated plants, (C) I control and (D) I IM-treated plants, and (E) HA89 (imidazolinone-susceptible) IM-treated plants. The center row shows photographs taken under stereomicroscope of (F–I) bud (E1) and (J–M) anthesis (E3) disc flowers from (F, J) R control and (G, K) IM-treated plants, and (H, L) I control and (I, M) IM-treated plants. The bottom row shows photographs taken under stereomicroscope of pollen grain viability tests. Blue-stained pollen grains are viable, but yellow pollen grains are unviable, from (N) R control, (O) R IM-treated, (P) I control, and (Q) I IM-treated plants. Scale bar = 50 μm.

and necrosis, and they finally died 20 d after treatment (Fig. 1E).

The stereomicroscope images obtained from bisexual disc flowers in E1 and E3 phenophases were analyzed to determine the sizes of female reproductive structures in the treated and control plants with the R and I genotypes (Fig. 1F–1I and 1J–1M, respectively). Total flower length, ovarian length, and ovarian width were measured and statistically compared by *t* test. The means and *p* values of statistical comparisons are shown in Table 1. Biometric data for disc flowers and ovaries show statistical significant differences between treated and control plants in only the bud flower phenophase (E1) in the I genotype.

## Quantitative and Qualitative Pollen Analysis

Clarified anthers from the flower buds of the R and I sunflower lines had two thecas containing masses of pollen grains in both treated and control plants (Fig. 2A–2D). Pollen grains per flower were estimated from closed anthers (E1 phenophase) in R and I genotypes. No statistically significant differences were detected between treated and control plants of the R genotype, but there was a significant decrease in pollen yield in treated plants of the I genotype. The treated plants had 27% less PGF than control plants. The means, SEs, and *p* values are provided in Table 1. Pollen viability was similar between the R and I genotypes (96.1 and 95.6%, respectively). Furthermore, there were no differences in the percentage of lacto-phenol-aniline blue-stained grains between IM-treated and control plants (Fig. 1N–1Q, Table 1).

The pollen grain diameter was analyzed by DIC microscopy (Fig. 2E–2H). No differences in the mean diameters were found when comparing the treated and control plants of the R genotype. However, we found that treated plants of the I genotype had pollen grains with significantly greater diameter (Table 1). Moreover, anthers in flower buds (E1 phenophase) revealed that both genotypes had large amounts of normal pollen grains, and no alterations or differences were detected in the anther morphology after IM treatment (Fig. 2A–2D). These results suggest that IM treatment alters the pollen grain formation of the I genotype, but it remains invariable in the R genotype. Moreover, we found that IM treatment does not induce anther malformation, and there was no

**Table 1. Biometric data of inbred sunflower lines HA425 and 1058-1: bisexual flowers (disc flowers), pollen grains, megagametophytes, and percentage of seed set. Means ± SE of parameters measured on control and treated plants of the imidazolinone (IMI)-resistant and IMI-intermediate-resistant genotypes are shown.**

| | IMI-resistant genotype (HA425) | | | IMI- Intermediate resistant genotype (1058-1) | | |
|---|---|---|---|---|---|---|
| Parameter† | Control | Treated | *p* | Control | Treated | *p* |
| Morphological variables | | | | | | |
| Disc flower length (mm), E1 | 12.58 ± 0.48 | 13.32 ± 0.39 | 0.26 | 12.77 ± 0.14 | 12.07 ± 0.13 | 0.009* |
| Ovarian length (mm), E1 | 3.58 ± 0.78 | 2.59 ± 0.10 | 0.26 | 5.27 ± 0.10 | 4.7 ± 0.14 | 0.19* |
| Ovarian width (mm), E1 | 4.47 ± 0.64 | 6.13 ± 0.36 | 0.06 | 2.6 ± 0.26 | 2.3 ± 0.1 | 0.068 |
| Disc flower length (mm), E3 | 21.28 ± 0.26 | 21.29 ± 0.27 | 0.98 | 20.5 ± 0.13 | 20.33 ± 0.23 | 0.66 |
| Ovarian length (mm), E3 | 10.02 ± 0.15 | 10.05 ± 0.17 | 0.95 | 8.60 ± 0.1 | 8.45 ± 0.1 | 0.39 |
| Ovarian width (mm), E3 | 3.46 ± 0.15 | 3.43 ± 0.09 | 0.89 | 2.96 ± 0.1 | 2.92 ± 0.1 | 0.99 |
| Pollen variables | | | | | | |
| Pollen grains per flower | 24.074 ± 1.32 | 25.66 ± 1.47 | 0.47 | 21.99 ± 1.07 | 16.06 ± 1.13 | <0.001* |
| Pollen viability (%) | 96.07 | 95.94 | 0.95 | 95.61 | 94.41 | 0.187 |
| Pollen diameter (μm) | 33.92 ± 0.38 | 33.69 ± 0.39 | 0.68 | 33.49 ± 0.33 | 36.17 ± 0.44 | <0.001* |
| Megagametophyte variable | | | | | | |
| Embryo sac length (μm), E1 | 269.76 ± 15.95 | 336.1 ± 6.83 | 0.007* | 315.69 ± 15.68 | 359.7 ± 8.93 | 0.006* |
| Embryo sac width (μm), E1 | 56.39 ± 8.35 | 80.09 ± 3.49 | 0.03* | 34.82 ± 5.40 | 42.36 ± 3.12 | 0.13 |
| N/En layer width (μm), E1 | 23.97 ± 1.16 | 16.91 ± 1.42 | 0.003* | 23.28 ± 2.45 | 23.44 ± 1.32 | 0.71 |
| Embryo sac length (μm), E3 | 469.02 ± 12.77 | 462.5 ± 15.77 | 0.71 | 502.65 ± 14.46 | 486.8 ± 18.8 | 0.29 |
| Embryo sac width (μm), E3 | 123.49 ± 3.46 | 120.58 ± 3.06 | 0.54 | 89.24 ± 5.81 | 86.17 ± 4.74 | 0.62 |
| N/En layer width (μm), E3 | 13.74 ± 1.43 | 16.44 ± 1.67 | 0.25 | 23.44 ± 1.61 | 12.74 ± 1.02 | 0.42 |
| Seed variable | | | | | | |
| Filled seeds (%) | 92.63 | 85.51 | 0.001* | 81.42 | 66.51 | <0.001* |

* Significant at the 0.05 probability level.

† E1 and E3 indicate the phenophases of the disc flowers. N/En indicates the nucellar and endothelium layers.

pollen viability differences either between R and I genotypes or between treated and control plants.

When we compared young anthers (11 d after IM treatment and the control) of immature flowers from the center of the disc of R and I genotypes, we did not find alterations in the archesporial cells inside de pollen sacs (Fig. 3A–3D). For the four treatment combinations, it was possible to visualize cell divisions. We can assume that the archespores mother cells are suffering meiotic reduction (see arrowheads). However, we found a rather different scenario in bisexual flowers from the periphery of the same disc of IM-treated anthers. After meiotic reduction, we expect to find clusters of microspores or individual microgametophytes. Although the confocal view of the right theca showed developed microspores with big and bright nucleous (Fig. 3E and 3F), left theca showed tissue damage, inferring cell death that might occur by apoptosis. The dark holes in the superior half of the theca indicated microspore damage (Fig. 3E).

## Megagametophyte Development

We used DIC microscopy to observe the megagametophytes of flower bud and flowers in anthesis of the R and I genotypes. The embryo sac cytology was analyzed in three different treated and control plants in both E1 and E3 phenophases. The mature sunflower ovule is anatropous, unitegmic, and tenuinucellate (Supplemental Fig. S1; Pullaiah, 1979). The observed embryo sacs were of the Polygonum type (Johri et al., 1992), had normal shapes, and were dimensioned according to their developmental stage without alterations in their cells (Fig. 2I–2P).

Most bud flowers in the E1 phenophase had ovules containing a young six-celled megagametophyte with an egg apparatus (the egg cell and two hooked synergids), a central cell, and two or three antipodals cells (Fig. 2I–2L). However, it is notable that the development of embryo sacs from treated plants was slightly advanced with respect to the control plants in the same phenological stage (Fig. 2J and 2L). Furthermore, some immature, narrow, and short embryo sacs were identified in E1 flowers of untreated plants, indicating that cell wall formation was incomplete (partial cytokinesis) and preventing the cells from being distinguished.

Mature embryo sacs were found in flower phenophase E3 (Fig. 2M–2P). Large megagametophytes with two synergides and one egg cell at the micropylar end were observed. The central cell, situated in the middle region between the micropylar and chalazal ends, showed abundant cytoplasm. The polar nuclei were already fused and formed a single nucleus located near the egg cell. In the chalazal region, two or three elongated antipodal cells with disorganized nuclei were linearly arranged in a transverse plane.

The embryo sacs were biometrically characterized by image analysis of the DIC micrographies. The embryo sac length, embryo sac width, and nucellar–endothelium

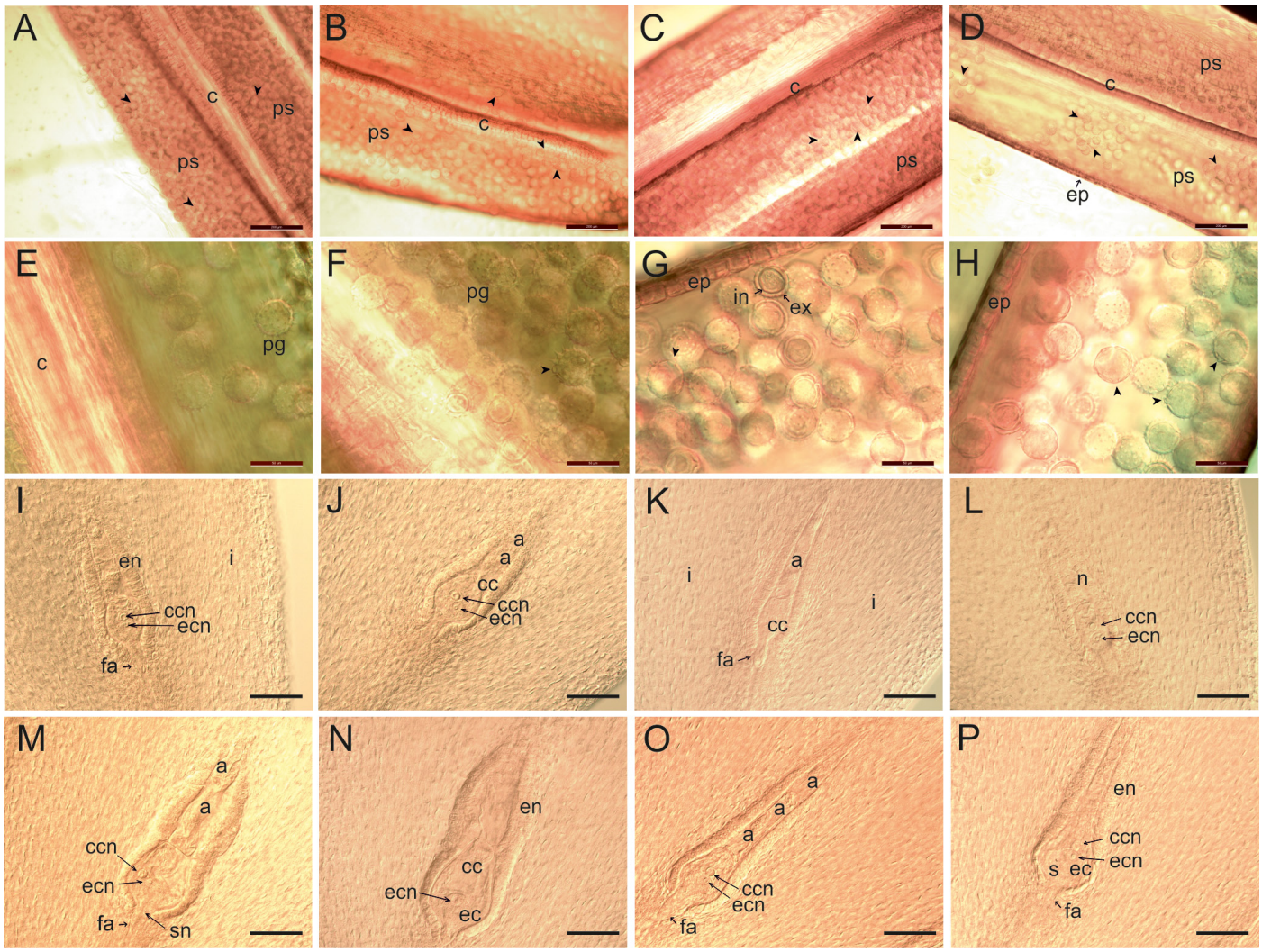


Fig. 2. Differential interference contrast micrographies of optical sections of anthers, pollen grains and embryo sacs from control and imazapyr-treated (IM-treated) plants of HA425 imidazolinone-resistant (R) and 1058-1 intermediate-resistant (I) genotypes. Panels A to D show anther views of (A) R control and (B) R IM-treated plants, and (C) I control and (D) I IM-treated plants. Thecas with two pollen sacs (ps) are joined by the connective tissue (c) containing masses of pollen grains (arrowhead). Photos also show the epidermis of the theca (ep). Scale bar = 200 μm. Panels E to H show pollen grains (pg) of (E) R control and (F) R IM-treated plants, and (G) I control and (H) I IM-treated (H) plants. In Panel G, it is possible to distinguish the epidermis (ep) of the theca, and the pollen grain exine (ex) and intine (in). Scale bar = 50 μm. Panels I to L show embryo sacs in E1 phenophase (flower bud) from (I) R control and (J) R IM-treated plants, and (K) I control and (L) I IM-treated plants. Photos show the mature embryo sac showing the filiform apparatus (fa), the egg cell nucleus (ecn), the central cell (cc) with the central cell nucleus (ccn), the antipodal cells (a), the nucellus (n), endotelium (en), and the integument (i). Scale bar = 100 μm. Panels M to P show embryo sacs in E3 phenophase (flower anthesis) of (M) R control and (N) R IM-treated plants, and (O) I control and (P) I IM-treated plants. Photos show the mature embryo sac showing the synergid (s) with the synergid nucleus (sn), the filiform apparatus (fa), the egg cell (ec) with the egg cell nucleus (ecn), the central cell (cc) with the central cell nucleus (ccn), the antipodal cells (a),the endothelium (en), and the nucellus (n). Scale bar = 100 μm

layer width were measured and statistically analyzed (Table 1). Significant differences among treatments were detected in only the reproductive phenophase E1. The embryo sac length was higher in treated plants from both genotypes, and embryo sac width was also higher in R treated plants, suggesting that IM treatment induced accelerated development. Nucellar–endothelium layer width was also significantly thinner in R treated plants, which supports the DIC observations that the development of embryo sacs of treated plants was advanced with respect to the control plants.

## Seed Analysis

The percentages of normally formed seeds were compared between treated and control plants from the R and I lines. Seed set percentages were significantly lower in IM-treated plants than in control plants from both the R and I genotypes, but these means differences were twice as high for the I genotype (Table 1). Treated plants of the I genotype had 14% fewer normal seeds than control plants, and treated plants of the R genotype had 7% reduced seed set compared with the control (Table 1).

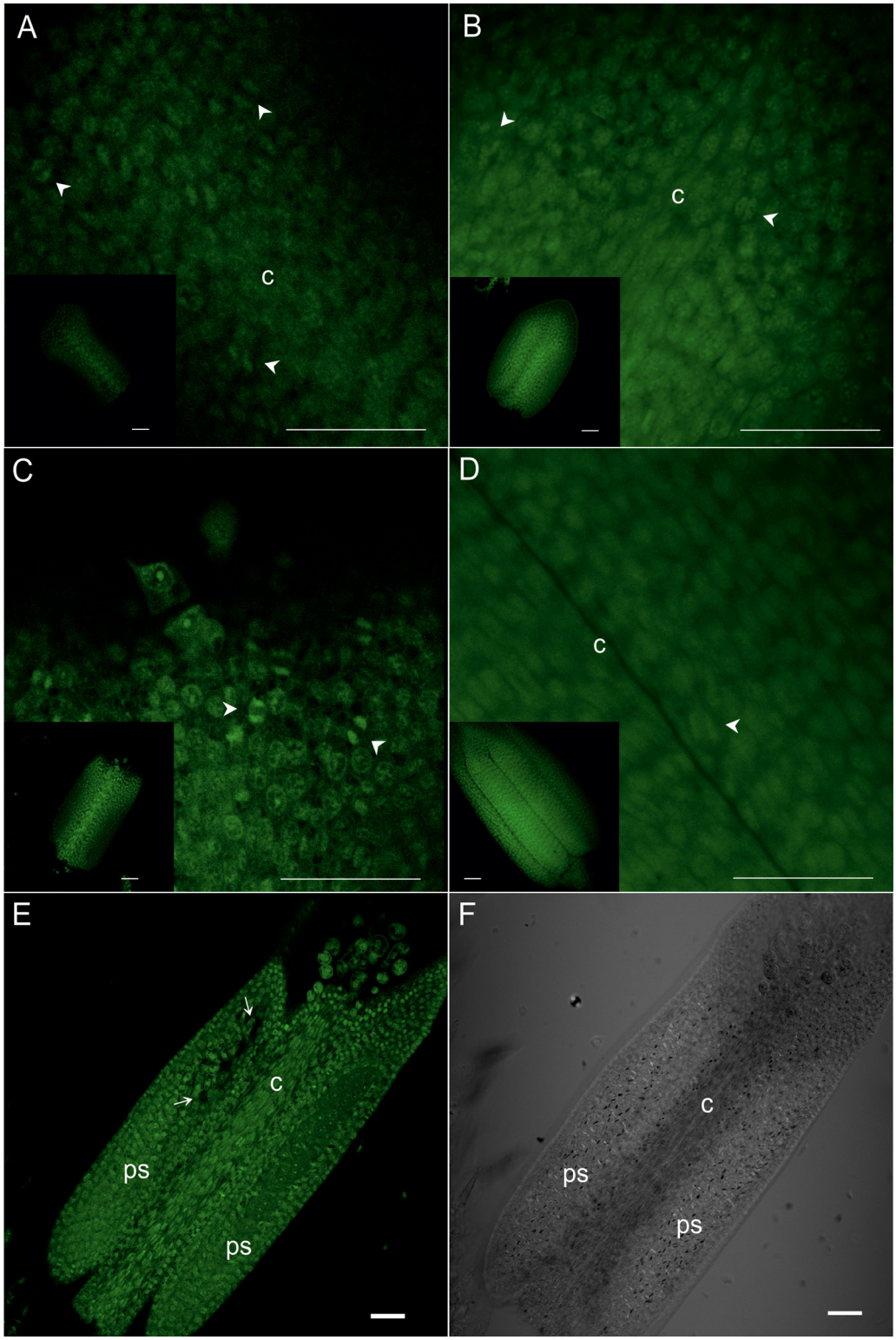


Fig. 3. Confocal laser micrographies of developing anthers from control and imazapyr-treated (IM-treated) plants of HA425 imidazolinone-resistant (R) and 1058-1 intermediate-resistant (I) genotypes. Panels A to D show confocal green fluorescence (488-nm line from a 40-mW Melles Griot argon ion laser and a 525/50 emission filter) of anthers of (A) R control and (B) R IM-treated plants, and (C) I control and (D) I IM-treated plants. Images represent the 80× magnification of anthers; sections and insets show the complete dissected anthers. Arrowheads show the meiotic structures during the microsporogenesis. Panels E and F show (E) the anther view obtained from a bisexual flower of the periphery of the disc of IM-treated plants in confocal green fluorescence (488-nm line, 525/50 emission filter) and (F) the differential interference contrast view of the same anther. In Panel E, thecas with two pollen sacs (ps) joined by the connective tissue (c) formed by long tabular cells between the two thecas. The right pollen sac with some cells still clustered, forming microspore tetrads, is also shown. Arrows indicate the abnormally developed or damaged sporogenous tissue. Scale bars = 50 μm.

## Effects of Imazapyr Treatment on the *ahas* Gene Profiles

Sunflower transcript profiles of the three *ahas* paralogs were analyzed through two different analysis strategies. First, each *ahas* gene expression level was independently studied to identify the maximum and minimum relative values within each paralog dataset by qBASE software (Hellemans et al., 2007; Fig. 4A, 4D, 4G, 4J, 4M, and 4P). Next, a statistical comparison of *ahas* expression between IM-treated and control plants and between E1 and E3 phenophases of both genotypes was assayed by REST software (Pfaffl et al., 2002; Fig. 4).

qBASE profiling analysis shows that the overall similarities between the R and I expression patterns were mainly for the *ahas1* gene. The highest expression levels of this gene were detected in the anthers in the E3 phenophase of control plants, with 18.12 and 16.2 times the expression of treated plants for the R and I genotypes, respectively (Fig. 4A and 4D). Divergent expression patterns were identified for *ahas2* and *ahas3* in both genotypes. Differences in *ahas2* levels in the R genotype were scarcely detected and were 2.97 times higher than the reference level in the preanthesis anthers of treated plants (E3 ovaries of treated plants, Fig. 4G).

A steeper variation was detected in control plants of the I genotype, where the highest level was detected in the E3 phenophase (49 times that of the E1 phenophase). However, such differences were not found in treated plants (Fig. 4J). The *Ahas3* paralog transcript amounts were also variable between genotypes. In R plants, the highest levels were detected in the bud flower anthers of treated plants (23.2 times higher than in the same tissues in anthesis) (Fig. 4M), but in the I genotype, the highest variations were observed in the anthers of treated plants and were 11 times higher in anthesis than in bud flowers (Fig. 4P). In the qBASE analysis, it should be noted that the main variations of the three *ahas* paralogs were detected almost exclusively in male reproductive tissues.

The REST analysis comprised the statistical comparison of *ahas* relative expression between IM-treated and control plants and also during the reproductive development (E1 and E3 phenophases) of both genotypes (Table 2). The expression levels of each *ahas* paralog were analyzed in female and male tissues separately, and the relative expression was calculated with respect to the lowest expression value within each tissue type. Herbicide treatment triggered significant changes at the transcriptional level of the three *ahas* genes, and the alterations were genotype dependent.

As described for the other comparison strategy, differences between the treated and control plants were mainly identified in male reproductive tissues (Fig. 4B, 4C, 4E, and 4F). *Ahas1* expression levels were no exception. Control plants had a sharp physiological incensement between E1 and E3 phenophase (11.2 and 16.2 times in R and I genotypes, respectively), but in IM-treated plants, transcript levels remained at a low constant level. This suggests that one or more other *ahas* paralogs are coding the principal isoform in male tissues under this stress condition. In E3 ovaries, significant differences were detected for the R genotype between treated and control plants, where IM treatment significantly increased the *ahas1* transcript level (Fig. 4B). However, divergent behavior was detected in the other genotype (I), since *ahas1* levels remained almost constant during normal ovary development but were initially induced but in IM-treated plants ($p = 0.029$) (Table 2).

In the *ahas2* expression analysis, significant variations between treated and control plants were detected in only the reproductive tissues of the E3 phenophase (Fig. 4H, 4I, 4K, and 4L). In ovaries of the R genotype, these paralog levels were slightly reduced after treatment (Fig. 4H). In the other genotype, the gene expression was three times lower in the E3 phenophase than in the E1 phenophase in control plants ($p = 0.001$), but when treated, the expression remained at a high and constant level (Fig. 4K). In the anthers of the R genotype, *ahas2* expression levels increased 2.4 times in IM-treated plants compared with control plants (Fig. 4I). Nonetheless, in the I genotype, these paralog transcripts were highly increased during normal male reproductive development ($p = 0.001$), but like *ahas1*, IM treatment negatively affected these levels (Fig. 4F). This suggests that AHAS2 could be one of the principal isoforms induced after IM treatment in female reproductive tissues of both genotypes, as well as in male tissues of the I genotype.

Finally, the relative transcript abundance of *ahas3* was analyzed (Fig. 4N, 4O, 4Q, and 4R). In female tissues, minimal but significant variations were detected in the R genotype between the E1 and E3 phenophases (a 0.7-fold decrease), and a similar pattern was observed in treated plants (Fig. 4N). In contrast, in the I genotype, *ahas3* levels were strongly induced by IM treatment in the E1 phenophase (37.3 times that of control plants) (Fig. 4Q). In the anthers of the R genotype, *ahas3* also had an initial significant induction of 4.5 times in the IM-treated plants compared with control plants ($p = 0.015$, Table 2).

In the I genotype, *ahas3* increased by three times between the E1 and E3 phenophases in control plants and by more than six times in IM-treated plants (Fig. 4R). Thus, *ahas3* has a constitutive behavior in female tissues of the R genotype, but in the I genotype, it could be induced by IM treatment in the early developmental stages. In bud flower anthers of the R genotype, there was a marked *ahas3* induction by IM treatment, but in the other genotype, this induction was detected in the anthesis. This suggests that the AHAS3 isoform could be one of the main components of the AHAS enzyme pool in male tissues of both genotypes and also in the ovaries of I plants exposed to herbicide treatment at the R1 stage.

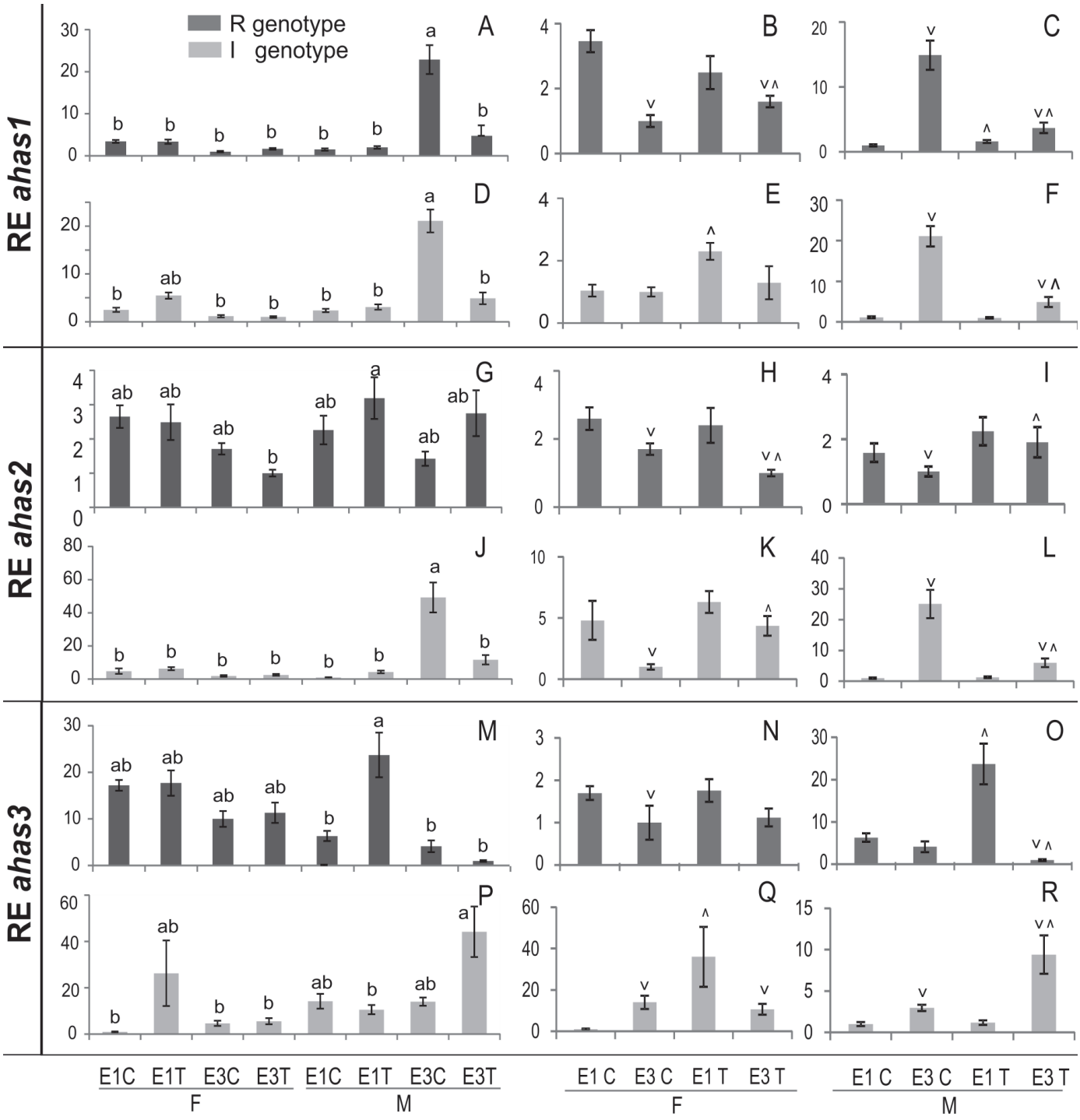


Fig. 4. Relative expression levels (RE) of the three sunflower ahas paralogs (ahas1, ahas2, and ahas3) measured in reproductive tissues of HA425 imidazolinone-resistant (R) and 1058-1 intermediate-resistant (I) genotypes. Expression profiles are shown of each ahas gene from R (A–D) and I (E–F) genotypes. Transcript levels were analyzed by two different strategies, referring them to the minimal gene expression of each comparative group. The vertical axis represents the RE, and vertical bars indicate the SE of the mean. Panels A and D show expression levels of each sample relative to the minimal normalized expression of the complete pool of samples from R and I genotypes, respectively. For each gene and genotype, samples with the same letter are not significantly different at the 0.05 probability level. F and M indicate Female and Male reproductive tissues, respectively. E1 and E3 are the phenological reproductive developmental stages, and T and C are control and imazapyr -treated plants, respectively. In Panels B, C, E, and F, expression data were statistically compared within each reproductive tissue type among developmental reproductive process and treatments. Panels B and E show the RE of ahas genes analyzed in the female tissue subgroup from R and I genotypes, respectively. Expression levels of ovaries in different phenophases (E1 and E3) and in treated (T) and control (C) plants were compared. Panels C and F show the RE of ahas genes analyzed in the male tissue subgroup from R and I genotypes, respectively. ˅ indicates significant mean differences between E1 and E3 phenophases ($p < 0.05$); ^ indicates significant mean differences between treated and control plants ($p < 0.05$). Table 2 provides the complete list of statistical analysis results.

Table 2. REST statistical analysis of *ahas* genes relative expression (RE) between imazapyr-treated (T) and control (C) plants and E1 and E3 developmental stages from imidazolinone-resistant (R) and intermediate-resistant (I) genotypes

| | | | | R | | I | |
|---|---|---|---|---|---|---|---|
| Gene | Tissue† | Stage‡ | Comparison | RE | *p* | RE | *p* |
| *ahas1* | F | E1 | T–C | NS§ | 0.54 | >1.92 | 0.029 |
| | F | E3 | T–C | >1.4 | 0.028 | NS | 0.52 |
| | F | C | E1–E3 | <0.21 | 0.001 | NS | 0.95 |
| | F | T | E1–E3 | <0.44 | 0.007 | NS | 0.16 |
| | M | E1 | T–C | >1.4 | 0.028 | NS | 0.54 |
| | M | E3 | T–C | <0.16 | 0.009 | <0.25 | 0.029 |
| | M | C | E1–E3 | >22.5 | 0.0001 | >13.4 | 0.01 |
| | M | T | E1–E3 | >2.55 | 0.011 | >4 | 0.03 |
| *ahas2* | F | E1 | T–C | NS | 0.83 | NS | 0.055 |
| | F | E3 | T–C | <0.54 | 0.03 | >3.7 | 0.012 |
| | F | C | E1–E3 | <0.63 | 0.001 | <0.23 | 0.001 |
| | F | T | E1–E3 | <0.33 | 0.022 | NS | 0.26 |
| | M | E1 | T–C | NS | 0.06 | NS | 0.46 |
| | M | E3 | T–C | >2.14 | 0.015 | <0.264 | 0.006 |
| | M | C | E1–E3 | <0.56 | 0.009 | >23 | 0.001 |
| | M | T | E1–E3 | NS | 0.207 | >4 | 0.03 |
| *ahas3* | F | E1 | T–C | NS | 0.75 | >27.9 | 0.001 |
| | F | E3 | T–C | NS | 0.63 | NS | 0.42 |
| | F | C | E1–E3 | <0.58 | 0.001 | >11.5 | 0.007 |
| | F | T | E1–E3 | NS | 0.116 | <0.23 | 0.001 |
| | M | E1 | T–C | >4.5 | 0.015 | NS | 0.53 |
| | M | E3 | T–C | <0.19 | 0.0001 | >2.7 | 0.003 |
| | M | C | E1–E3 | NS | 0.26 | >3 | 0.016 |
| | M | T | E1–E3 | <0.027 | 0.007 | >6 | 0.012 |

† F and M are female and male reproductive tissues, respectively.

‡ E1 and E3 are immature and mature reproductive developmental stages, respectively.

§ NS indicates nonsignificant differences ($p > 0.05$).

## DISCUSSION

Overall, our study demonstrated that the number of PGF and the percentage of viable seeds are significantly decreased by IM treatment in early reproductive growth stages. This decrease is dependent on the level of resistance of the genotype, since the PGF was significantly decreased by the IM treatment in only the I genotype, and the number of viable seeds was twice as low in this genotype than in the R genotype. Likewise, the pollen diameter was increased in treated plants in only the I genotype. Nevertheless, the anther morphology development was normal, and no loss of pollen viability was detected in treated plants.

These results suggest that the IMI treatment alters the pollen yield. This has an adverse effect on the pollen–ovule relationship and affects seed production, particularly in the genotype lacking the modifier gene *Imr2*. Additionally, in this genotype, the average of pollen grain diameter was significantly increased by the IMI treatment. *Helianthus annuus* is an allogamous species that presents a SSI mechanism similar to other species in Asteraceae (Gerstel, 1950; Hughes and Babcock, 1950; Allen et al., 2011). Most species with SSI have been found to correlate with trinucleate pollen grains as the anthers open.

This study evaluated the anther morphology, pollen structure, and PGF in flower phenophase E1 with the anthers closed before dehiscence. It is possible that pollen grains were still at the two-cell stage (binucleate) in the E1 phenophase, which means that the generative cells of the microgametophytes would not have undergone mitosis yet. Higashiyama and Inatsugi (2006) pointed out that the genes regulating the timing of division of the generative cell are still unknown, although water uptake may trigger the division of the generative cells in bicellular pollen. During microgametogenesis, sunflower binucleate pollen grains undergo a second mitosis before anther dehiscence. Given these events, it could be assumed that the significant increase in pollen grains diameter in E1 flowers in plants of the I genotype correspond to an advanced developmental stage of the microgametophyte.

It is possible that flowers from treated plants of the I genotype were undergoing a precocious second mitosis of the microgametophyte generative cells. However, it seems that there could be another possible explanation for the significantly increased pollen grain diameter in the I treated plants. Johri et al. (1992) mentioned that pollen degeneration is a common feature in several members of Asteraceae, and they found that with larger sized pollen grains occasionally undergo the process of becoming binucleate and then posteriorly abort. Nevertheless, we did not observe shrinking or deformed pollen grains that suggest the idea of cell death in phenophases E1 or E3.

When the flower length and ovarian length from treated plants were compared with control plants in the E1 flower developmental stage, significantly smaller structures were observed in only treated plants of the I genotype. However, treated plants of both genotypes showed longer embryo sacs than the control, suggesting that the megagametophytes of these flowers could have been in an advanced developmental phase. These results indicate that the IMI treatment not only accelerates the gametogenesis in the pollen grains of treated plants of the I genotype but also affects the embryo sac length in both genotypes.

The decrease in pollen yield indicates that the negative effect of the herbicide treatment could occur in the initial phases of microgametogenesis. Notwithstanding, the number of pollen grains do not seem to be the only determining factor for the decrease of the seed set, since the number of normal seeds was significantly reduced by the treatment in the R genotype, but the PGF was not affected at all. As mentioned, the megagametophyte development were especially affected by IM treatment in the R genotype, since biometric differences in the embryo sac were mainly detected for this genotype between treated and control plants. This suggests that different mechanisms would be involved in the reduction of seed yield in R and I genotypes under IM treatment.

Herbicide treatment triggered significant changes in the transcriptional profile of the three *ahas* genes, and these alterations were also genotype dependent. The main variations of *ahas* paralog levels were detected in male reproductive tissues, but transcript profiles were altered by IM treatment in all evaluated reproductive tissues. Overall, the gene expression analyses showed that the R genotype had a restricted response to treatment. In this genotype, IM treatment slightly induced *ahas1* levels in ovaries of the E3 phenophase, and the other two paralogs appeared to have a constitutive expression, suggesting that the three paralogs could be coding the enzyme pool, but AHAS1 could be overexpressed in this stress condition.

In male tissues, a compensative expression profile was detected where IM treatment induced *ahas3* in early developed flowers, but in maturity, it hardly induced *ahas2* expression and reduced *ahas1* and *ahas3* levels. Thus, these results suggest that in the R genotype, AHAS2 and AHAS3 are the principal treatment-induced isoforms in the anthers during anthesis and in bud flowers, respectively. A marked effect of IM treatment was detected for the I genotype, where *ahas1* and *ahas3* expression levels were highly induced in early developed ovaries, as well as *ahas2* levels in ovaries of the E3 phenophase. In this genotype, unlike R, AHAS1 and AHAS3 could be the principal isoforms that responded to the treatment in female reproductive tissue. During anther development, the treatment barely suppressed *ahas1* and *ahas2* but induced *ahas3* expression, suggesting that AHAS3 could be the principal isoform in anthers of the I genotype.

In a previously published study (Ochogavía et al., 2014), we demonstrated that AHAS2 and AHAS3 are the principal isoforms in reproductive tissues of the HA89 IMI-susceptible sunflower line (wild type). A positive correlation has been established between *ahas2* and *ahas3* gene expression and AHAS activity for these tissues. The paralog *ahas1* is mainly expressed in vegetative tissues, and thus the enzyme pool in flowers of this wild-type genotype had the lowest contributions of the AHAS1 isoform (Ochogavía et al., 2014). In our comparison, both the R and I genotypes carried the *Ahasl1-1* allele (Ala205 mutation). It has been demonstrated for other plant species (*Solanum ptychanthum* Dunal) that this mutation reduces the specific AHAS activity to 50%, and it is related to the fitness cost of the resistance (Ashigh and Tardif, 2007; Vila-Aiub et al., 2009). Different expression patterns between *ahas* mutants and wild-type genotypes were expected, since higher transcriptional levels may compensate for the reduced functionality of this isoform (Lee et al., 2011).

We demonstrated that the herbicide response was not uniform for the two genotypes evaluated. The effective herbicide action probably differed because R and I genotypes differ in their herbicide resistance level. The *Imr2* locus has been related to a non-target-site resistance mechanism associated with P450s isozymes (Breccia et al., 2017). Recently, Balabanova et al. (2018) showed that GSTs enzymes are also involved in imazamox detoxification in the sunflower Imisun trait and thus contribute to its non-target-site resistance. Thus, different behaviors between genotypes were expected, as this mechanism is only present in the R genotype. The earlier and higher induction of *ahas1* in female reproductive structures of the I genotype after treatment could be associated with a major effort in the plant to counteract the increasing concentration of herbicide that reaches the affected tissues. In the same way, the significant physiological effects detected in IMI-treated anthers were expected, since the *ahas1* paralog had an important inhibition effect in these tissues, particularly for the I genotype.

Some AHAS-inhibiting sulfonylureas herbicides, such as tibenuron methyl and monosulfuron ester sodium, have been used as effective chemical hybridization agents to induce male sterility in rapeseed. Underlying molecular bases have been proposed involving sulfonylurea causing anther-specific inhibition of AHAS and subsequent BCAA starvation, which induces autophagic cell death in the anthers (Zhao et al., 2015). Foliar-sprayed tibenuron methyl is polar transported to the anthers through the mesophyll and phloem, producing anther-specific AHAS inhibition in *Brassica napus* and *Arabidopsis* (Zhao et al., 2015). Autophagic cell death is induced by BCAA starvation, and the bulk cytoplasmic contents in aborted microspores are degraded,

resulting in extremely crinkled pollen grains with little cytoplasm, and ultimately, male sterility.

During autophagic cell death, the bulk cytoplasmic contents in aborted cells are degraded, with microspores and tapetum cells highly vacuolated (Zhao et al., 2015). It is possible that analogous biochemical or metabolic pathways are altered after IM treatment in sunflower. More detailed studies on microsporogenesis and microgametogenesis should be done for Imisun genotypes to identify evidence of autophagic events in the anther cells of IM-treated plants. Our study provides clear evidence that IM treatment in the R1 stage induces significant negative effects in pollen production (i.e., pollen yield reduction in only the I genotype), as well as a decrease in normal seed production (7 and 14% in the R and I genotypes, respectively).

A tissue-specific and gene-dependent response was also observed in this study. The highest variations were detected almost exclusively in the anthers. The significant reduction in *ahas1* and induction of the other paralogs after treatment reveal an IM-induced compensative expression in anthers, which is particularly marked in the I genotype. This suggests that AHAS2 and AHAS3 were the principal isoforms that led to BCAA synthesis in altered male tissues after the herbicide treatment. Our results underscore the functional links between IMI treatment in early reproductive growth stages and the decrease of seed production, which is directly related to crop yield. Finally, this study specially contributes to enhancing the understanding of the molecular effects of AHAS-inhibitors herbicides in reproductive tissues. The broader knowledge about the mechanism underlying this chemical male sterilization constitutes a requisite for the implementation of this promising method in breeding schemes or in the production of hybrid seeds.

## Conflict of Interest

The authors declare that they have no conflict of interest.

## Supplemental Material Available

Supplemental material for this article is available online.

### Acknowledgments

Thanks are due to Dr. Jerry Miller and to Dr. José María Bruniard for kindly gifting seed materials. Financial support from the Fondo para la Investigación Científica y Tecnológica (PICT 2013 1010 and PICT 2016 1316) and Consejo Nacional de Investigaciones Científicas y Técnicas (PUE 0043) is also acknowledged.

### References

Abramoff, M.D., P.J. Magalhaes, and S.J. Ram. 2004. Image processing with ImageJ. Biophotonics Int. 11:36–42.

Allen, A.M., C.J. Thorogood, M.J. Hegarty, C. Lexer, and S.J. Hiscock. 2011. Pollen–pistil interactions and self-incompatibility in the Asteraceae: New insights from studies of *Senecio squalidus* (Oxford ragwort). Ann. Bot. (Lond.) 108:687–698. doi:10.1093/aob/mcr147

Ashigh, J., and F. Tardif. 2007. An ala205val substitution in acetohydroxyacid synthase of eastern black nightshade (*Solanum ptychanthum*) reduces sensitivity to herbicides and feedback inhibition. Weed Sci. 55:558–565. doi:10.1614/WS-07-054.1

Astiz, V., L.A. Iriarte, A. Flemmer, and L.F. Hernández. 2011. Self-compatibility in modern hybrids of sunflower (*Helianthus annuus* L.). Fruit set in open and self-pollinated (bag isolated) plants grown in two different locations. Helia 34:129–138. doi:10.2298/hel1154129a

Balabanova, D., T. Remans, A. Vasilev, A. Cuypers, and J. Vangronsveld. 2018. Possible involvement of glutathione S-transferases in imazamox detoxification in an imidazolinone-resistant sunflower hybrid. J. Plant Physiol. 221:62–65. doi:10.1016/j.jplph.2017.12.008

Breccia, G., M. Gil, T. Vega, E. Altieri, M. Bulos, L. Picardi, and G. Nestares. 2017. Contribution of non-target-site resistance in imidazolinone-resistant Imisun sunflower. Bragantia 76:4. doi:10.1590/1678-4499.2016.336

Breccia, G., G. Vega, S. Felitti, L. Picardi, and G. Nestares. 2013. Differential expression of acetohydroxyacid synthase genes in sunflower plantlets and its response to imazapyr herbicide. Plant Sci. 208:28–33. doi:10.1016/j.plantsci.2013.03.008

Bruniard, J.M., and J.F. Miller. 2001. Inheritance of imidazolinone-herbicide resistance in sunflower. Helia 24:11–16.

Duggleby, R., J.A. Mccourt, and L.W. Guddat. 2008. Structure and mechanism of inhibition of plant acetohydroxyacid synthase. Plant Physiol. Biochem. 46:309–324. doi:10.1016/j.plaphy.2007.12.004

Gerstel, D.U. 1950. Self-incompatibility studies in guayule II. Inheritance. Genetics 35:482–506.

Gressel, J., and L.A. Segel. 1978. The paucity of plants evolving genetic resistance to herbicides: Possible reasons and implications. J. Theor. Biol. 75:349–371. doi:10.1016/0022-5193(78)90340-5

Heiser, C.B., D.M. Smith, S.B. Clevenger, W.C. Martin, Jr. 1969. The North American sunflowers (*Helianthus*). Mem. Torrey Bot. Club 22:1–218.

Hellemans, J., G. Mortier, A. De Paepe, F. Speleman, and J. Vandesompele. 2007. qBase relative quantification framework and software for management and automated analysis of real-time quantitative PCR data. Genome Biol. 8:R19. doi:10.1186/gb-2007-8-2-r19

Herr, J.M., Jr. 1971. A new clearing-squash technique for the study of ovule development in angiosperms. Am. J. Bot. 58:785–790. doi:10.1002/j.1537-2197.1971.tb10031.x

Higashiyama, T., and R. Inatsugi. 2006. Comparative analysis of biological models used in the study of pollen tube growth. In: R. Malhó, editor, The pollen tube: A cellular and molecular perspective. Springer, Berlin, Heidelberg. p. 265–286. doi:10.1007/7089_053

Hiscock, S.J., and S.M. McInnis. 2003. Pollen recognition and rejection during the sporophytic self incompatibility response: Brassica and beyond. Trends Plant Sci. 8:606–613. doi:10.1016/j.tplants.2003.10.007

Hofgen, R., B. Laber, I. Schuttke, A. Klonus, W. Streber, and H. Pohlenz. 1995. Repression of acetolactate synthase activity through antisense inhibition: Molecular and biochemical analysis of transgenic potato (*Solanum tuberosum L.* cv *Desiree*) plants. Plant Physiol. 107:469–477. doi:10.1104/pp.107.2.469

Hughes, M.B., and E.B. Babcock. 1950. Self-incompatibility in *Crepis foetida* (L.) subsp. *rhoeadifolia* (Bieb.) Schinz et Keller. Genetics 35:570–588.

Johri, B.M., K.B. Ambegeokar, and P.S. Srivastava. 1992. II Dicotyledons: Sympetalae, 5.1 Compositae. In: B.M. Johri, et al., editors, Comparative embriology of angiosperms. Vol. 2. Springer-Verlag, Berlin, Heidelberg. p. 809–822.

Kearns, C.A., and D.W. Inouye. 1993. Techniques for pollination biologists. Univ. Press of Colorado, Niwot.

Kolkman, J.M., M.B. Slabaugh, J.M. Bruniard, S. Berry, B.S. Bushman, C. Olungu, et al. 2004. Acetohydroxyacid synthase mutations conferring resistance to imidazolinone or sulfonylurea herbicides in sunflower. Theor. Appl. Genet. 109:1147–1159. doi:10.1007/s00122-004-1716-7

LaRossa, R.A., and J. Schloss. 1984. The sulfonylurea herbicide sulfometuron methyl is an extremely potent and selective inhibitor of acetolactate synthase in Salmonella typhimurium. J. Biol. Chem. 259:8753–8757.

Lee, H., S. Rustgi, N. Kumar, I. Burke, J.P. Yenish, K.S. Gill, et al. 2011. Single nucleotide mutation in the barley acetohydroxy acid synthase (AHAS) gene confers resistance to imidazolinone herbicides. Proc. Natl. Acad. Sci. USA 108:8909–8913. doi:10.1073/pnas.1105612108

Leica Microsystems. 2009. Leica application suite LAS version 4.6.2 (Build 210). Leica Microsyst., Wetzlar, Germany.

Lersten, N.R., and J.D. Curtis. 1988. Secretory reservoirs (ducts) of two kinds in giant ragweed (*Ambrosia trifida*; Asteraceae). Am. J. Bot. 75:1313–1323. doi:10.1002/j.1537-2197.1988.tb14192.x

Mallory-Smith, C.A., D.C. Thill, and J.M. Dial. 1990. Identification of sulfonylurea herbicide-resistant prickly lettuce (*Lactuca serriola*). Weed Technol. 4:163–168. doi:10.1017/S0890037X00025173

Maneval, W.E. 1936. Lacto-phenol preparations. Stain Technol. 11:9–11. doi:10.3109/10520293609111316

Miller, J.F., and K. Al-Khatib. 2002. Registration of imidazolinone herbicide-resistant sunflower maintainer (HA 425) and fertility restorer (RHA 426 and RHA 427) germplasms. Crop Sci. 42:988–989. doi:10.2135/cropsci2002.988a

Nikon Corporation. 2009. Nikon EZ-C1 Gold version 3.90 (Build 869). Nikon Corp., Tokyo.

Ochogavía, A.C., G. Breccia, T. Vega, S.A. Felitti, L.A. Picardi, and G. Nestares. 2014. Acetohydroxyacid synthase activity and transcripts profiling reveal tissue-specific regulation of ahas genes in sunflower. Plant Sci. 224:144–150. doi:10.1016/j.plantsci.2014.04.018

Ochogavía, A.C., M.A. Novello, L. Picardi, and G. Nestares. 2017. Identification of suitable reference genes by quantitative real-time PCR for gene expression normalization in sunflower. Plant Omics J. 10:210–218. doi:10.21475/poj.10.04.17.pne831

Pfaffl, M.W., G.W. Horgan, and L. Dempfle. 2002. Relative expression software tool (REST©) for group-wise comparison and statistical analysis of relative expression results in real-time PCR. Nucleic Acids Res. 30:e36. doi:10.1093/nar/30.9.e36

Pullaiah, T. 1979. Embryology of *Adenostemma, Elephantopus* and *Vernonia* (Compositae). Bot. Not. 132:51–56.

QIAGEN. 2008. Rotor-Gene Q Series software 1.7 (Build 94). Corbett Life Sci., a QIAGEN company, Hilden, Germany.

R Development Core Team. 2013. R: A language and environment for statistical computing. Version 3.0.0. R Found. Stat. Comput., Austria.

Ray, T. 1984. Site of action of chlorsulfuron. Plant Physiol. 75:827–831. doi:10.1104/pp.75.3.827

Sala, C.A., and M. Bulos. 2012. Use of imidazolinone tolerance to produce male-sterile testers in sunflower breeding programs. In: Proceedings of 18th International Sunflower Conference, Mar del Plata, Argentina. 27 Feb.–1 Mar. 2012. Vol. 1. Int. Sunflower Assoc., Paris. Paper 174.

Sala, C.A., M. Bulos, E. Altieri, and M.L. Ramos. 2012. Genetics and breeding of herbicide tolerance in sunflower. Helia 35:57–70. doi:10.2298/HEL1257057S

Sala, C.A., M. Bulos, M. Echarte, S.R. Whitt, and R. Ascenzi. 2008. Molecular and biochemical characterization of an induced mutation conferring imidazolinone resistance in sunflower. Theor. Appl. Genet. 118:105–112. doi:10.1007/s00122-008-0880-6

Schneiter, A.A., and J.F. Miller. 1981. Description of sunflower growth stages. Crop Sci. 21:901–903. doi:10.2135/cropsci1981.0011183X002100060024x

Singh, B.K., and D.L. Shaner. 1995. Biosynthesis of branched chain amino acids: From test tube to field. Plant Cell 7:935–944. doi:10.1105/tpc.7.7.935

Tan, S., R. Evans, and B. Singh. 2006. Herbicidal inhibitors of amino acid biosynthesis and herbicide-tolerant crops. Amino Acids 30:195–204. doi:10.1007/s00726-005-0254-1

Tranel, P.J., and T.R. Wright. 2002. Resistance to ALS-inhibiting herbicides: What have we learned? Weed Sci. 50:700–712. doi:10.1614/0043-1745(2002)050[0700:RROWTA]2.0.CO;2

Vila-Aiub, M.M., P. Neve, and S.B. Powles. 2009. Fitness costs associated with evolved herbicide resistance alleles in plants. New Phytol. 184:751–767. doi:10.1111/j.1469-8137.2009.03055.x

Zhao, L., X. Jing, L. Chen, Y. Liu, Y. Su, T. Liu, et al. 2015. Tribenuron-methyl induces male sterility through anther-specific inhibition of acetolactate synthase leading to autophagic cell death. Mol. Plant 8:1710–1724. doi:10.1016/j.molp.2015.08.009